

# Perception Helps Planning: Facilitating Multi-Stage Lane-Level Integration via Double-Edge Structures

Guoliang You<sup>1</sup>, Xiaomeng Chu<sup>1</sup>, Yifan Duan<sup>1</sup>, Wenyu Zhang<sup>1</sup>, Xingchen Li<sup>1</sup>, Sha Zhang<sup>1</sup>, Yao Li<sup>1</sup>, Jianmin Ji<sup>1,2</sup>, Yanyong Zhang<sup>1,2</sup>, Fellow, IEEE

**Abstract**— When planning for autonomous driving, it is crucial to consider essential traffic elements such as lanes, intersections, traffic regulations, and dynamic agents. However, they are often overlooked by the traditional end-to-end planning methods, likely leading to inefficiencies and non-compliance with traffic regulations. In this work, we endeavor to integrate the perception of these elements into the planning task. To this end, we propose Perception Helps Planning (PHP), a novel framework that reconciles lane-level planning with perception. This integration ensures that planning is inherently aligned with traffic constraints, thus facilitating safe and efficient driving. Specifically, PHP focuses on both edges of a lane for planning and perception purposes, taking into consideration the 3D positions of both lane edges and attributes for lane intersections, lane directions, lane occupancy, and planning. In the algorithmic design, the process begins with the transformer encoding multi-camera images to extract the above features and predicting lane-level perception results. Next, the hierarchical feature early fusion module refines the features for predicting planning attributes. Finally, the double-edge interpreter utilizes a late-fusion process specifically designed to integrate lane-level perception and planning information, culminating in the generation of vehicle control signals. Experiments on three Carla benchmarks show significant improvements in driving score of 27.20%, 33.47%, and 15.54% over existing algorithms, respectively, achieving the state-of-the-art performance, with the system operating up to 22.57 FPS.

**Index Terms**—End-to-End Planning, Autonomous Driving.

## I. INTRODUCTION

Autonomous driving [1] plays a vital role in improving the efficiency and safety of transportation systems, intersecting the fields of computer vision and robotics [2]–[5]. A key challenge lies in devising safe and efficient path planning [6], which must account for various traffic elements such as lane restrictions, intersections, and directions, along with the occupancy of agent. Planning algorithms in autonomous driving can be broadly categorized into two types: rule-based planning [7]–[10] and end-to-end learning-based planning [11]–[16]. Traditional rule-based planning uses complex algorithms such as BEV-LaneDet [8] for lane detection and BevFormer [7] to predict the positions of vehicles and pedestrians, followed by optimization techniques like RRT [9] to find safe paths, with high computational cost. On the other hand, end-to-end planning, demonstrated by NVIDIA [12],

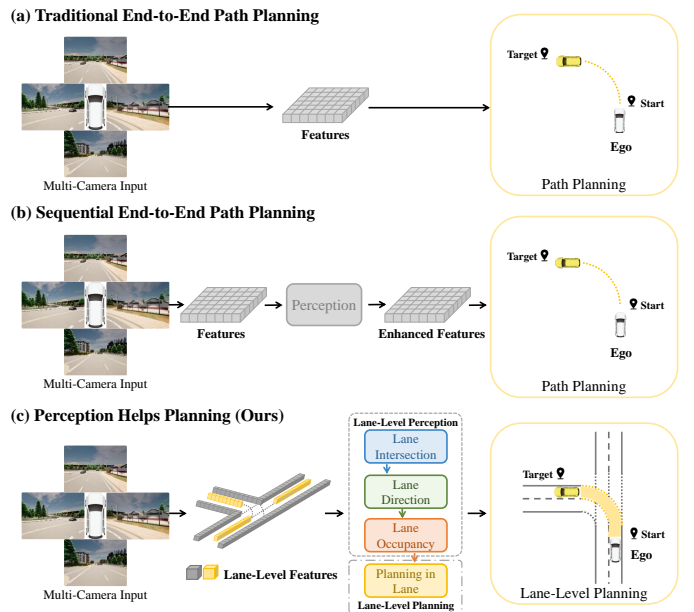


Fig. 1: Comparison of Autonomous Driving Framework: a) Traditional end-to-end framework prioritizes planning policy optimization without considering perception. b) Sequential integration framework enhance planning by incorporating perception into traditional end-to-end planning, but lack interaction between perception and planning. c) Our Perception Helps Planning (PHP) framework transform path planning as lane-level task, integrating multi-level lane-centric perception at both the feature and result levels.

maps raw pixels to steering via CNNs, cutting computational needs. However, its efficiency comes at the cost of limited perception of complex environments, affecting planning precision. To address the perception limitations in traditional end-to-end models, a variant approach exemplified by the ST-P3 algorithm [14] implements a sequential strategy. It enhances Bird’s Eye View (BEV) representations from multi-cameras using spatiotemporal modules, subsequently utilizing these representations in planning modules. Despite this, such algorithms inadequately leverage the potential synergy between perception and planning. This leads to a fragmented integration of the two processes, thereby constraining the performance.

Given these challenges, the question arises: is it feasible to develop an algorithm that smoothly integrates perception and planning? In response, we propose PHP, a framework where the double-edge data structure facilitates the transformation from path planning to lane-level planning, integrating

<sup>1</sup> School of Computer Science and Technology, University of Science and Technology of China (USTC), Hefei 230026, China

<sup>2</sup> School of Artificial Intelligence and Data Science, University of Science and Technology of China (USTC), Hefei 230026, China

<sup>†</sup> Corresponding author. yanyongz, jianmin@ustc.edu.cn

lane-level perception task within it. Additionally, to predict elements within the double-edge structure, we designed a transformer-based method that utilizes early fusion at the feature-level and late fusion at the result-level. This approach strengthens the collaboration between perception and planning components within the double-edge data structure.

Specifically, the double-edge data structure encapsulates five component of traffic elements: 3D position for each lane edge and attributes for lane intersection, lane direction, lane occupancy and planning. By abstracting traffic information into these components, double-edge captures both the dynamic and static properties of traffic scenario. In algorithm, it first encodes features from multi-camera, then employs a double-edge transformer to achieve feature embedding for each double-edge component, and utilizes 3D position, intersection, direction, and occupancy branches to predict these components. Subsequently, a hierarchical feature early fusion module, based on these feature embedding, enhances the relevance of features for planning. In addition, to improve the guidance ability of the target point, we vectorize the target point, guiding the prediction of planning attribute. Finally, an interpreter decodes double-edge data, converting and fusion perception and planning at the result-level into control signals for vehicle.

This work demonstrates the feasibility of planning at the lane level. It achieves synchronous lane-level perception and planning by deeply integrating both aspects. This integration ensures that planning strategies adhere to traffic regulations and adapt to real-time changes in perception. In the Carla [17] benchmark, extensive tests on Perception Helps Planning (PHP) confirmed its ability to ensure safety across traffic scenarios and achieve state-of-the-art performance.

In summary, our main contributions are as follows:

- We introduce the PHP, a novel lane-level planning framework that transforms path planning into lane-level planning. PHP integrates perception with planning and ensuring planning compliance with traffic rules.
- We develop a algorithm that extracts double-edge component features from multi-camera images, integrating early-fusion of features level with late-fusion of result-level to significantly enhance safety and efficiency.
- We conducted experiments on three benchmarks, where PHP outperformed previous algorithms with driving score improvements of 27.20%, 33.47%, and 15.54%, and up to 22.57 FPS, achieving state-of-the-art performance.

## II. RELATE WORK

In this section, we provide an overview of rule-based planning algorithms [2], [3], [5], [6], [18] and end-to-end learning-based planning algorithms in autonomous driving [11].

**Traditional Rule-based Planning Algorithm.** Traditional rule-based algorithms integrate perception and planning, forming the navigation systems. The perception accurately models the environment. It employs Simultaneous Localization and Mapping (SLAM) algorithms [19]–[21] to enable autonomous systems to construct and update environmental maps and determine their positions within these maps. Camera-based 3D object detection techniques [7], [22]–[25] identify, recognize

and locate objects, enriching the environmental model. Lane detection algorithms [8], [26]–[28] delineate traffic constraints by detecting lanes, contributing to the environmental model. Based on the environmental model provided by the perception, planning employs search-based algorithms such as Rapidly Exploring Random Trees (RRT) and its variants [9], [29]–[31], along with the A Star (A\*) search algorithm [32], to plan a safe path to the destination. These algorithms take advantage of perception data for safe and efficient path planning.

**End-to-End Learning-based Planning Algorithms.** End-to-end planning aim to simplify system by using neural networks to directly output planning policies, such as path or steering control signals. The initial methodologies directly predicted these policies [12], [13], [33]–[35], sidestepping the environmental perception and understanding, leading to limited performance and interpretability. Such as, NVIDIA [12] used the camera as input to train a neural network that directly outputs control signals. LBC [34] utilized mimicking techniques to train image networks with supervision from a privileged model. To mitigate these drawbacks, variants of end-to-end methods integrate perception into planning sequentially or as auxiliary tasks [14]–[16], [36]–[42]. This integration enhances the planning system’s environmental comprehension, which improves performance. In this context, NEAT [16] introduced neural attention fields for infusing reasoning capabilities into end-to-end driving models. ST-P3 [14] proposes a spatial-temporal feature learning scheme to generate more representative features for perception, prediction, and planning.

## III. METHODOLOGY

### A. Overall Framework

As depicted in Figure 2, PHP introduces a novel method that smoothly integrates perception and planning at the lane level. At the core of PHP is the double-edge data structure, which encapsulates the 3D positions of each lane edges (double-edge 3D), lane-level attributes (i.e., intersection and direction), and point-level attributes (i.e., occupancy and planning). This structure facilitates a new planning paradigm, transforming path planning into lane-level planning. In algorithm, the transformer for double-edge planning design a double-edge query for efficient double-edge feature retrieval. Based on double-edge feature, it decodes 3D positions of each lane edges via double-edge 3D regression branch, while also extracting intersections, direction, and occupancy features for hierarchical feature fusion and predicting these attributes through the corresponding branches. The hierarchical feature early fusion module employs attention mechanisms to fusion intersection, direction, and occupancy features, enriching the planning feature with a thorough understanding of traffic scenario. The target-guided planning branch uses cross attention to enhance the dynamic responsiveness of the planning feature to target points, thus improving planning accuracy. Lastly, the double-edge interpreter translates the combined perception and planning data into vehicle control signals.

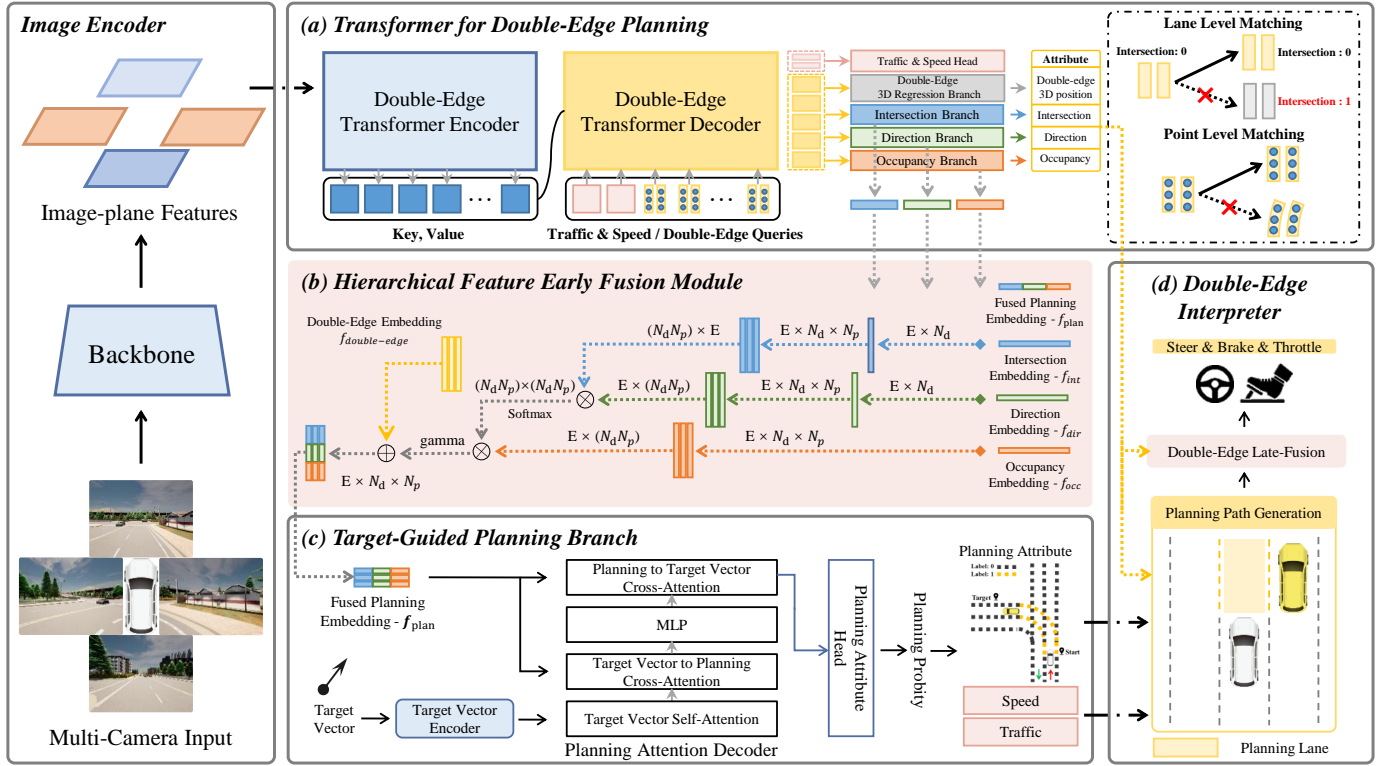


Fig. 2: The PHP framework begins with a image encoder. (a) The encoded image is processed by the transformer for double-edge planning, achieving double-edge component features, and predicting 3D position of lane edges and related attributes. (b) These features are fused in the hierarchical feature early fusion module using an attention mechanism. (c) The target-guided planning branch enhances the interaction between the target point and fused features for prediction of planning attributes. (d) Finally, the double-edge interpreter fuses and transforms the perception and planning information at the result level into control signals. The symbol  $\oplus$  represents point-wise addition, while  $\otimes$  denotes matrix multiplication.

### B. Double-Edge Data Structure

We define  $N_d$  double-edge data ( $l_d^i$ ) that incorporate lane and point-level traffic information to describe environment  $L$ :

$$L = \{l_d^i\}_{i=0}^{N_d}, \quad (1)$$

$$l_d^i = (edge_l^i, edge_r^i, int_i, dir_i),$$

$$int_i = \{0 \text{ or } 1\}, dir_i = \{0 \text{ or } 1\},$$

where  $l_d^i$  includes the lane's left and right  $edges_i$ , along with its lane-level intersection  $int_i$  and direction  $dir_i$  attributes. Within the double-edge,  $int_i$  and  $dir_i$  indicate whether a lane is an intersection and if the lane's direction is aligned with the direction of the ego vehicle's travel respectively.  $edge^i$  encompasses 3D point and attributes for corresponding points, including occupancy and planning attributes that indicate the point level. Each  $edge$  consists of  $\frac{N_p}{2}$  elements, defined as:

$$edge^i = \{point^j, occ^j, plan^j\}_{j=0}^{\frac{N_p}{2}}, \quad (2)$$

$$point^j = \{x, y, z\}, occ^j = \{0 \text{ or } 1\}, plan^j = \{0 \text{ or } 1\},$$

where  $occ^j$  and  $plan^j$  indicate whether the lane is occupied by traffic agents (e.g., pedestrians, vehicles) and whether it is selected for planning. In Figure 3,  $point^j$  illustrates the location of edge using dashed and solid lines to represent lane-level and point-level visualizations, respectively. Gray denotes attribute values of zero, while blue, green, orange, and yellow indicate a value of one, visualizing different properties of

double-edge. In Figure 3, i shows blue identifying lanes are intersections, green in ii as lanes adhering to ego vehicle travel direction, orange in iii highlighting point in lane unoccupied by pedestrian and vehicle, and yellow in iv as point selected for planning. Double-edge transforms path planning into a lane-level task, allowing concurrent perception and planning.

### C. Transformer for Double-Edge Planning

To acquire lane-level features that support the learning of lane-level perception and planning tasks, we have incorporated the transformer, applying a double-edge query to learn double-edge lane-level features, as depicted in Figure 2(a).

**Double-edge transformer encoder.** Initially, for each image input  $\mathbf{I} \in \mathbb{R}^{3 \times H_0 \times W_0}$ , we employ a ResNet-50 [43] to extracting features  $\mathbf{f} \in \mathbb{R}^{C \times H \times W}$ . The values for  $C$ ,  $H$ , and  $W$  are defined as  $C = 256$ ,  $H = \frac{H_0}{32}$ , and  $W = \frac{W_0}{32}$ . The dimension of the transformer hidden layer is  $E$ . For each feature  $\mathbf{f}$ , the double-edge transformer encoder applies a 11 convolution to generate a lower-channel feature  $\mathbf{z} \in \mathbb{R}^{E \times H \times W}$ . Next, we simplify the spatial dimensions of  $\mathbf{z}$  into a sequence, forming  $E \times HW$  tokens. A fixed sinusoidal positional encoding  $\mathbf{e} \in \mathbb{R}^{E \times HW}$  is then added to each token to preserve positional information within each sensor input:

$$\mathbf{v}_i^{(x,y)} = \mathbf{z}_i^{(x,y)} + \mathbf{e}^{(x,y)}, \quad (3)$$

where  $\mathbf{z}_i$  represents the tokens extracted from the  $i$ -th view, and  $x$  and  $y$  denote the token's coordinate index in that sensor.

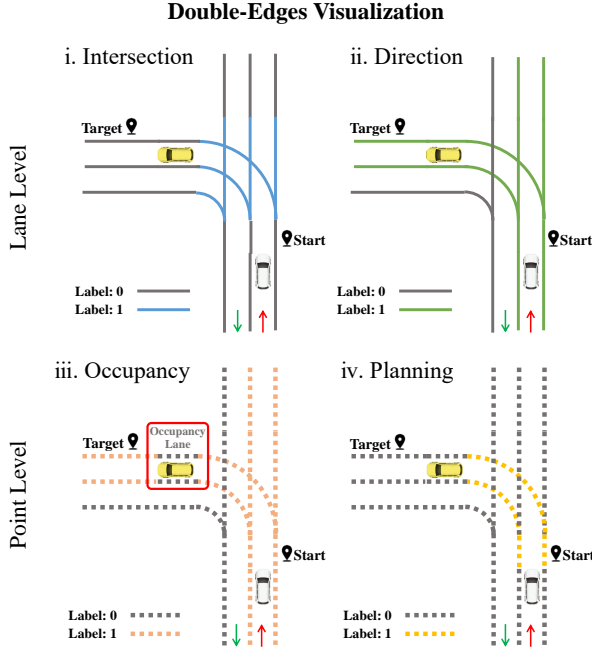


Fig. 3: Visualizes double-edge in a traffic scenario  $L$ , with blue and green detailing lane level attributes for intersections and directions. orange and yellow detail point-level attributes, marking unoccupied and selected planning lane.

Finally, we concatenate the tokens from all sensors and pass them through a transformer encoder comprising  $K$  standard transformer layers. Each layer  $K$  consists of Multi-Headed Self-Attention, MLP blocks, and layer normalization.

**Double-edge transformer decoder.** The double-edge transformer decoder's key function is to query the double-edge features using  $K$  layers multi-head self-attention, which are used to predict double-edge 3D and attributes for intersection, direction, and occupancy. We have designed multiple double-edge query  $q_{double-edge} \in \mathbb{R}^{E \times N_p}$ , to query lane-level double-edge features. A total of  $N_d$  such queries are deployed, as shown in Figure 4. Additionally, we introduce the speed query  $q_s \in \mathbb{R}^{E \times 1}$  and traffic query  $q_t \in \mathbb{R}^{E \times 1}$  to query the maximum speed  $Plan_{speed}$  allowed on the lane selected by planning attribute and to perceive traffic signals, respectively. In addition, based on double-edge features, we have devised a double-edge 3D regression branch capable of predicting the 3D points within the double-edge, with size  $N_d \times N_p \times 2$ . We then processed the double-edge features through three different feature extraction and attribute prediction branches to achieve prediction results for intersection ( $N_d \times 1$ ), direction ( $N_d \times 1$ ), and occupancy ( $N_d \times N_p \times 1$ ). Throughout this process, we preserve these features of intersection  $f_{int} \in \mathbb{R}^{E \times N_d}$ , direction  $f_{dir} \in \mathbb{R}^{E \times N_d}$ , occupancy  $f_{occ} \in \mathbb{R}^{E \times N_d \times N_p}$ , and double-edge  $f_{double-edge} \in \mathbb{R}^{E \times N_d \times N_p}$ , laying the foundation for the hierarchical lane fusion module.

#### D. Hierarchical Feature Early Fusion Module

Figure 2(b) introduces the hierarchical feature early fusion module, which effectively integrates both dynamic and static traffic information through attention at lane and point levels, thereby enabling a more detailed understanding of

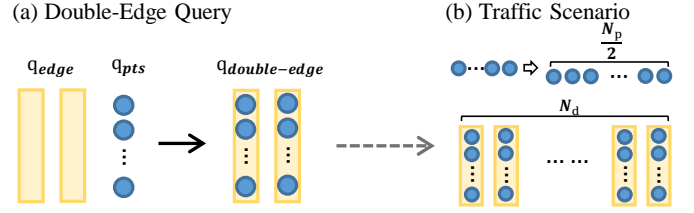


Fig. 4: (a) Each double-edge query  $q_{double-edge}$  consists of pair of edge query,  $q_{edge}$ , each edge query comprising a set of query points,  $q_{pts}$ . (b) A scenario features  $N_d$  such  $q_{edge}$  pairs, and each lane within a  $q_{edge}$  contains  $\frac{N_p}{2}$  query points.

traffic scenes. First, we extend intersection and direction embedding across  $N_d$  dimensions at the lane level, achieving dimensions of  $E \times N_d \times N_p$ . This is because each point within a double-edge shares identical intersection and direction attributes. Next, we multiply the intersection embedding with the direction embedding to form a feature matrix  $f_{int2dir} \in \mathbb{R}^{N_d N_p \times N_d N_p}$ . This multiplication integrates intersection and direction attributes at the lane level, defined as:

$$f_{int2dir} = R(f_{int}, [E, N_d N_p])^T \odot R(f_{dir}, [E, N_d N_p]), \quad (4)$$

where  $R$  denotes reshape operation. Subsequently, We convert the feature matrix  $f_{int2dir}$  into a probability matrix via softmax, quantifying the significance of each feature.

Then, to integrate point-level occupancy embedding, we obtain the feature matrix  $f_{fusion} \in \mathbb{R}^{E \times N_d N_p}$  by performing pointwise multiplication between this probability matrix and the occupancy embedding. This operation serves as an attention, highlighting occupancy embedding relevant to intersection and direction lane, thus focusing on compliant intersections and lane direction areas,  $f_{fusion}$  is defined as:

$$f_{fusion} = R(f_{occ}, [E, N_d N_p]) \odot \text{Softmax}(f_{int2dir}). \quad (5)$$

Finally, by integrating the matrix  $f_{fusion}$  with the double-edge embedding  $f_{double-edge}$ , we obtain the fused planning embedding  $f_{plan} \in \mathbb{R}^{E \times N_d \times N_p}$ , which improves understanding of static and dynamic information for prediction. This integration employs weighted fusion, controlled by a learnable parameter  $gamma$ , which dictates the fusion degree between the original and new features.  $f_{plan}$  is defined as:

$$f_{plan} = R(f_{fusion}, [E, N_d, N_p]) \times gamma + f_{double-edge}. \quad (6)$$

#### E. Target-Guided Planning Branch

We aim to assist autonomous driving systems in selecting the optimal planning lane, guided by a specified target point. To accomplish this, we introduce a target vector encoder and a planning attention decoder, as shown in Figure 2(c). The target vector encoder,  $Encoder_{vector}$ , encodes the target point,  $Point_t$ , into a target vector embedding. It then applies position embeddings from random spatial distributions, transforming spatial coordinates into a higher-dimensional target vector embedding  $f_{vector}$ . This enables more effective extraction and utilization of destination position information by the model. It can be formulated as:

$$f_{vector} = Encoder_{vector}(Point_t). \quad (7)$$

The planning attention decoder starts with target vector self-attention (TSA) on the encoded target vector embedding  $f_{vector}$ , followed by target vector to planning cross-attention (TPCA) on the planning embedding, which is then processed through a multilayer perceptron (MLP). Subsequently, planning to target vector cross-attention (PTCA) amplifies the most relevant planning embedding,  $F_{plan}$ , to the target vector. It enhances the planning embedding's ability to highlight the relevant features for the target vector.  $F_{plan}$  is formulated as:

$$F_{plan} = \text{PTCA}(\text{MLP}(\text{TPCA}(\text{TSA}(f_{vector}), f_{plan})), f_{plan}), \quad (8)$$

where TPCA enhances planning features relevant to the target vector through cross-attention, PTCA reinforces this relevance with additional cross-attention. These stages effectively capture information relevant to the target points within the planning embedding. Finally, the planning attribute head processes the amplified embedding  $F_{plan}$  to predict the probability of planning attributes ( $N_d \times N_p \times 1$ ) within the double-edge.

### F. Double-Edge Interpreter

The double-edge interpreter integrates planning path generation and double-edge late-fusion for safer navigation.

**Planning Path Generation.** Firstly, we use left and right edge points in double-edge to reconstruct lane information and assign attributes. These attributes include intersection and direction for lane level and occupancy and planning for point level, as shown in Figure 3. Second, we select edge points within double-edge marked by planning attribute value of '1' (indicating suitability for planning) to construct the path:

$$Plan_{path} = \bigcup_{j=1}^{N_d \times \frac{N_p}{2}} \left\{ \frac{point_l^j + point_r^j}{2} \mid plan_l^j, plan_r^j = 1 \right\}. \quad (9)$$

**Double-Edge Late-fusion.** To leverage the perceived traffic information—intersection, direction, and occupancy—in the double-edge, we efficiently integrate this information using a late-fusion strategy to enhance safety. Initially, direction filters out non-compliant occupancy data, focusing on lanes adhering to traffic regulations. We then assess each double-edge occupancy attribute through the planning attribute at the point level. When the planning attribute is '1' and occupancy is '0' (signifying traffic participants within planning lanes), the respective planning path is marked as a stopping path, represented  $Path_{stop}$ . In addition, if the planning path length is '1', indicating an extremely short path, we classify this path as a stopping path to ensure safety, indicating an immediate need for avoidance action. It can be formulated as:

$$Plan_{stop} = \begin{cases} True, & \text{if } plan^j = 1, occ^j = 0 \\ True, & \text{if } length(Plan_{path}) = 1. \\ False, & \text{Otherwise} \end{cases} \quad (10)$$

Finally, the planning path ( $Plan_{path}$ ), speed ( $Plan_{speed}$ ), and stop information ( $Plan_{stop}$ ) are integrated as trajectory inputs to the Model Predictive Control (MPC) [44] for generating control commands. With integration, the double-edge interpreter ensures safety and enhances interpretability.

$$Trajectory = [Plan_{path}, Plan_{speed}, Plan_{stop}]. \quad (11)$$

### G. Loss Function

Loss function includes the double-edge alignment cost and double-edge prediction loss based on these results.

**Double-Edge Alignment Cost.** We aim to determine optimal alignment  $\hat{\pi}$  between predicted and ground truth double-edge for training. This involves aligning the predicted intersection attribute  $\hat{v}_i$  with its ground truth  $v_i$ , and the predicted double-edge 3D  $\hat{p}_i$  with the ground truth  $p_i$ , defined as:

$$\hat{\pi} = \arg \min_{\pi \in \prod_{i=0}^{N_d-1}} \sum_{i=0}^{N_d-1} \{ \alpha L_{lane}(\hat{v}_{\pi(i)}, v_i), \beta L_{point}(\hat{p}_{\pi(i)}, p_i) \}, \quad (12)$$

$$L_{lane} = - \sum_{j=0}^{N_{gt}-1} \log(\hat{v}_j) [v_j], \quad (13)$$

$$L_{point} = \frac{1}{N_{gt}} \sum_{i=0}^{N_{gt}-1} \sum_{j=0}^{\frac{N_p}{2}-1} \{ |\hat{p}_{ij}^l - p_{ij}^l| + |\hat{p}_{ij}^r - p_{ij}^r| \}, \quad (14)$$

where  $L_{lane}$  and  $L_{point}$  represent lane and point level alignment, and  $N_{gt}$  indicates successful matches with ground truth double-edges, and in training,  $\alpha$  and  $\beta$  are in a 5:2 ratio.

**Double-Edge Prediction Loss.** Following the optimal alignment result, we train for perception and planning to predict double-edges. These include: (1)  $L_{edge\_3d}$  for double-edge 3D regression, (2)  $L_{int}$  and (3)  $L_{dir}$  for intersection and direction respectively at the lane level, and (4)  $L_{occ}$  and (5)  $L_{plan}$  for occupancy and planning respectively at the point level. Additionally,  $L_{speed}$  and  $L_{signal}$  are used for predicting planning speed and traffic signals. Formulated as:

$$Loss = \gamma L_{edge\_3d} + \delta L_{int} + \epsilon L_{dir} + \varepsilon L_{occ} + \zeta L_{plan} + \eta L_{speed} + \theta L_{signal}, \quad (15)$$

where, in training,  $\gamma$ ,  $\delta$ ,  $\epsilon$ ,  $\varepsilon$ ,  $\zeta$ ,  $\eta$  and  $\theta$  are set to 5:2:1:3:4:1:0.1.  $L_{edge\_3d}$  and  $L_{plan}$  can be formulated as:

$$L_{edge\_3d} = \frac{1}{N_{gt}} \sum_{i=0}^{N_{gt}-1} \sum_{j=0}^{\frac{N_p}{2}-1} \{ |\text{pred}_{ij}^l - gt_{ij}^l| + |\text{pred}_{ij}^r - gt_{ij}^r| \}, \quad (16)$$

$$L_{plan} = \sum_{i=0}^{N_{gt}-1} \sum_{j=0}^{\frac{N_p}{2}-1} \left\{ \frac{(\rho \cdot (1 - e^{-CE(\text{pred}_{ij}, gt_{ij})}))^2 \cdot CE(\text{pred}_{ij}, gt_{ij})}{D_{point2target}} \right\}, \quad (17)$$

where  $D_{point2target}$  represents the distance from a edge point in double-edge to the target vector, serving as weights to emphasize planning features near target points, and  $\rho$  is to 0.25. In addition,  $L_{int}$ ,  $L_{dir}$ , and  $L_{occ}$  employ Focal Loss [45], while  $L_{speed}$  uses SmoothL1Loss [46], and  $L_{signal}$  is based on Cross-Entropy Loss.

## IV. EXPERIMENTS

### A. Implementation Details

**Dataset and Metrics.** Using autonomous driving environment Carla [17], we gather 126K frames from diverse scenarios across 8 maps and 13 weathers. The data are collected at 2Hz with vehicles equipped with four cameras, an IMU, and a GPS. And, we annotate 3D edge points with attributes including



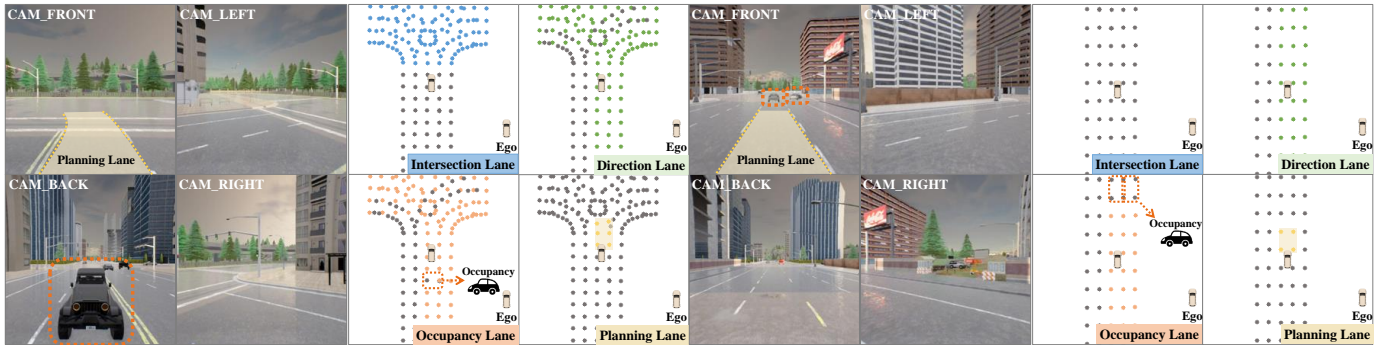


Fig. 5: Visualization of PHP includes multi-camera images and double-edges, showcasing lane intersections, lane direction, occupancy lanes, and selected lanes for planning. planning lanes are highlighted on the front camera.

TABLE I: Performance Comparison on Carla Town05.

Method	Town05 Short		Town05 Long	
	DS $\uparrow$	RC $\uparrow$	DS $\uparrow$	RC $\uparrow$
CILRS [33]	7.47	13.40	3.68	7.19
LBC [34]	30.97	55.01	7.05	32.09
ST-P3 [14]	55.14	86.74	11.45	83.15
VAD [42]	64.29	87.26	30.31	75.20
NEAT [16]	58.70	77.32	37.72	62.13
WOR [36]	64.79	87.47	44.80	82.41
Roach [40]	65.26	88.24	43.64	80.37
<b>PHP (ours)</b>	<b>92.46</b>	<b>97.04</b>	<b>78.27</b>	<b>96.16</b>
<b>Impro. (%)</b>	<b>+27.20</b>	<b>+8.80</b>	<b>+33.47</b>	<b>+13.01</b>

TABLE II: Performance Comparison on Carla 42 Routes.

Method	Carla 42 Routes		
	DS $\uparrow$	RC $\uparrow$	IS $\uparrow$
CILRS [33]	22.97	35.46	0.66
LBC [34]	29.07	61.35	0.57
AIM [39]	51.25	70.04	0.73
TransFuser [41]	53.40	72.18	0.74
NEAT [16]	65.17	79.17	0.82
Roach [40]	65.08	85.16	0.77
WOR [36]	67.64	90.16	0.75
<b>PHP (ours)</b>	<b>83.18</b>	<b>94.02</b>	<b>0.89</b>
<b>Impro. (%)</b>	<b>+15.54</b>	<b>+3.86</b>	<b>+7.00</b>

intersection, direction, occupancy, and planning. Driving Score (DS), Route Completion (RC), and Infraction Score (IS) as key metrics evaluating performance, where higher scores reflect better progress, safety, and rule adherence.

**Component Details.** We scale  $800 \times 600$  images to  $224 \times 224$  and process them using ResNet-50 for the transformer, with settings:  $N_d = 30$ ,  $N_p = 20$ , 6 layers each for the encoder and decoder. In the hierarchical feature early fusion, features are fused and fed into the target-guided planning branch, where the target vector and planning embeddings are processed with an attention decoder (feature dimension: 256, hidden layer: 128).

### B. Performance on Carla Benchmark

In this section, we evaluate PHP’s performance across three benchmarks: Town05 long, Town05 short, and Carla 42 Routes, which challenge autonomous driving algorithms with diverse urban and rural settings, dynamic objects, and varying weather. The benchmarks range from complex urban environments to village roads, including features like highways and roundabouts. Comparative results with state-of-the-art **vision-based algorithms** are presented in Tables I and II.

**Driving Score.** The Driving Score (DS) comprehensively assesses autonomous driving systems performance, combining route completion and infraction scores. In the Town05 Long, Short, and Carla 42 Routes benchmarks, PHP excels over other algorithms, achieving the highest DS scores. Specifically, in the Town05 benchmarks, our system achieves a DS improvement of 27.20% (Short) and 33.47% (Long), as detailed in Table I. Additionally, in the Carla 42 Routes Benchmark, a notable 15.54% increase in DS score is observed, as in Table II. These results underscore the effectiveness of our approach in enhancing planning safety and traffic regulation compliance.

**Route Completion.** Route Completion (RC) is a critical metric for assessing an autonomous driving system’s success in completing predetermined routes throughout the evaluation process, reflecting the system’s ability to plan routes and accurately understand target points. In the Carla Town05 and Carla 42 Routes benchmark, our method, by integrating planning with perception, improves its understanding of the traffic environment and target points, demonstrating exceptional route completion capabilities and achieving the highest scores. Compared to other algorithms, our method shows a higher route completion rate in benchmark tests that included a diverse range of urban and rural environments. Specifically, on the Carla Town05 Short and Long benchmarks, our method achieves improvements of 8.80% and 13.01%, respectively, as shown in Table I. Additionally, on the Carla 42 Routes benchmark, which features a variety of scenarios, our method also achieves an improvement of 3.86%, as indicated in Table II. These results highlight our method’s advanced capabilities in route planning and target point understanding, as well as its robustness in adapting to different road conditions.

**Infraction Score.** Infraction Score (IS) is a comprehensive metric used to evaluate systems performance, including avoiding collisions, adhering to traffic rules, and handling complex situations. PHP exhibits significant performance in Carla 42 Routes, achieving an 7.00% enhancement in Infraction Score (IS) as detailed in Table II, surpassing other algorithms.

### C. Qualitative Results

In Figure 5, we illustrate our system’s (PHP) ability to hierarchically perceive the traffic environment and seamlessly integrate planning tasks at the lane level. The visualization includes intersection lanes marked in blue, direction lanes

TABLE III: Ablation study on Carla Town01, Town05 and 42 Routes. "TGP" denotes target-guided planning, "HEF" denotes hierarchical feature early fusion, and "DLF" denotes the double-edge late-fusion enabled in the double-edge interpreter.

ID.	TGP	HEF	DLF	Carla Town01			Town05 Short			Town05 Long			Carla 42 Routes			
	% $\uparrow$	Sec III-E	Sec III-D	Sec III-F	RC	DS	IS	RC	DS	IS	RC	DS	IS	RC	DS	IS
A		✗	✗	✗	25.09	19.86	72.00	27.05	23.82	88.80	10.86	7.99	58.90	32.41	14.63	49.40
B		✓	✗	✗	86.89	47.02	51.90	81.85	54.85	67.70	74.96	22.99	26.20	86.12	59.99	68.70
C		✓	✓	✗	88.57	75.64	83.10	90.17	75.85	84.10	81.86	43.63	51.50	90.74	70.35	76.90
D		✓	✓	✓	<b>90.20</b>	<b>87.48</b>	<b>96.00</b>	<b>97.04</b>	<b>92.46</b>	<b>95.10</b>	<b>96.16</b>	<b>78.27</b>	<b>81.30</b>	<b>94.02</b>	<b>83.18</b>	<b>89.00</b>

that indicate roads complying with traffic regulations marked in green, and occupancy lanes for roads unoccupied by traffic agent and adhering to direction marked in orange. The planning lane, highlighted in yellow, signifies the optimally chosen lane that ensures safety and leads to the target point. In addition, we include camera images from four perspectives.

#### D. Ablation Studies

**Impact of Target-Guided Planning Branch:** In PHP, analyzing the correlation between traffic environment information and target points can significantly enhance decision accuracy and routing completion. The target-guided planning branch (TGP) deepens understanding of this correlation, optimizing decision-making. The TGP identifies key planning features related to target vector, strengthening their decision-making role. Experiment B, using TGP, the RC metric shows increases of 61.80%, 54.80%, 64.10%, and 53.71% over Experiment A, as shown in Table III. This underscores the TGP module's effectiveness in guiding decisions and the value of understanding the correlation between target vector and planning features. This approach improves the accuracy and route completion by aligning decisions with the target vector.

**Impact of Hierarchical Feature Early Fusion Module:** Although the introduction of the TGP in PHP improves route completion, it also highlights a limitation: the planning features' inability to fully comprehend environmental, leading to a reduction in infraction score. The inclusion of the TGP and the Hierarchical Early Fusion (HEF) module in Experiment C led to noticeable improvements in both infraction and driving scores. When compared with Experiment B, the infraction scores increased by 31.20%, 16.40%, 25.30%, and 8.20%. The driving scores also increased by 28.62%, 21.00%, 20.64%, and 10.36%, as shown in Table III. This indicates that optimizing planning through TGP alone is insufficient; it is necessary to enhance environmental understanding through modules like HEF to achieve a deep integration of planning and perception. The core of HEF lies in its ability to understand the environment hierarchically and explore the correlations between multiple layers of perception for attention fusion, significantly improving the environmental perception capabilities related to planning. Since planning tasks are constrained by perception, the safety of planning is further enhanced. This underscores the importance of deeply integrating planning and perception.

**Impact of Double-Edge Interpreter:** In PHP, the planning path generation interprets road geometry, traffic, and planning attributes from double-edges, converting them into planning paths. This process is indispensable. The double-edge late-fusion (DLF) module, an additional late-fusion module, enhances safety by leveraging perception and planning information. It late-fuses this information from double-edge data

TABLE IV: Efficiency and Performance of the PHP.

Method	Latency (ms) $\downarrow$	FPS $\uparrow$
ST-P3 [14]	476.74	2.1
TransFuser [41]	171.93	5.82
NEAT [16]	85.08	11.75
VAD [42]	59.50	16.81
<b>PHP (ours)</b>	<b>44.30</b>	<b>22.57</b>

to avoid hazardous planning, thus improving safety. Experiment D validates the effectiveness of DLF in coordinating perception and planning, with infraction score increases of 12.90%, 11.0%, 29.80%, and 12.10% compared to Experiment C, which lacked DLF. This strategy extracts safety-related information from intersection, direction, occupancy, and planning attributes, significantly lowering infraction rates and improving driving performance.

**Efficiency of PHP:** At the core of PHP's innovation is the design of the double-edge data structure, which confines planning and perception tasks to the lane space, significantly reducing computational cost. The effectiveness of this integrated approach is underscored by a significant decrease in total inference time to 44.30 ms and an impressive frame rate of approximately 22.57 FPS, as shown in Table IV.

## V. CONCLUSION

In this paper, we propose Perception Helps Planning (PHP), a novel framework that innovatively integrates planning with perception tasks at the lane level. Distinct from previous efforts, PHP employs a double-edge data structure to transform path planning into a lane-level task, embedding the planning process deeply within perception tasks. This unique strategy not only enables simultaneous traffic perception and planning within lanes but also ensures that the planning approaches are thoroughly compliant with traffic regulations. Moreover, this integration significantly improves efficiency and ensures adherence to traffic regulations, thereby enhancing safety and reliability. Experiments on Carla Benchmark demonstrate the effectiveness of the proposed method, which outperforms the state-of-the-art vision-based end-to-end planning algorithms.

## REFERENCES

- [1] C. Badue, R. Guidolini, R. V. Carneiro, P. Azevedo, V. B. Cardoso, A. Forechi, L. Jesus, R. Berriel, T. M. Paixao, F. Mutz *et al.*, "Self-driving cars: A survey," *Expert Systems with Applications*, vol. 165, p. 113816, 2021.
- [2] R. Qian, X. Lai, and X. Li, "3d object detection for autonomous driving: A survey," *Pattern Recognit.*, vol. 130, p. 108796, 2022.
- [3] X. Li, Y. Xiao, B. Wang, H. Ren, Y. Zhang, and J. Ji, "Automatic targetless lidar-camera calibration: a survey," *Artificial Intelligence Review*, vol. 56, no. 9, pp. 9949–9987, 2023.
- [4] W. Yu, J. Peng, H. Yang, J. Zhang, Y. Duan, J. Ji, and Y. Zhang, "Ldp: A local diffusion planner for efficient robot navigation and collision avoidance," *arXiv preprint arXiv:2407.01950*, 2024.

- [5] M. U. Khan, S. A. A. Zaidi, A. Ishtiaq, S. U. R. Bukhari, S. Samer, and A. Farman, "A comparative survey of lidar-slam and lidar based sensor technologies," in *2021 Mohammad Ali Jinnah University International Conference on Computing (MAJICC)*. IEEE, 2021, pp. 1–8.
- [6] B. Paden, M. Čáp, S. Z. Yong, D. Yershov, and E. Frazzoli, "A survey of motion planning and control techniques for self-driving urban vehicles," *IEEE Transactions on intelligent vehicles*, vol. 1, no. 1, pp. 33–55, 2016.
- [7] Z. Li, W. Wang, H. Li, E. Xie, C. Sima, T. Lu, Y. Qiao, and J. Dai, "Bevformer: Learning bird's-eye-view representation from multi-camera images via spatiotemporal transformers," in *Computer Vision - ECCV 2022 - 17th European Conference, Tel Aviv, Israel, October 23-27, 2022, Proceedings, Part IX*, ser. Lecture Notes in Computer Science, vol. 13669. Springer, 2022.
- [8] R. Wang, J. Qin, K. Li, Y. Li, D. Cao, and J. Xu, "Bev-lanedet: An efficient 3d lane detection based on virtual camera via key-points," in *Proceedings of the IEEE/CVF Conference on Computer Vision and Pattern Recognition*, 2023, pp. 1002–1011.
- [9] S. M. LaValle, "Rapidly-exploring random trees: A new tool for path planning," 1998.
- [10] A. Tahirovic and M. Ferizbegovic, "Rapidly-exploring random vines (rvv) for motion planning in configuration spaces with narrow passages," in *2018 IEEE International Conference on Robotics and Automation (ICRA)*. IEEE, 2018.
- [11] P. S. Chib and P. Singh, "Recent advancements in end-to-end autonomous driving using deep learning: A survey," *IEEE Transactions on Intelligent Vehicles*, 2023.
- [12] M. Bojarski, D. Del Testa, D. Dworakowski, B. Firner, B. Flepp, P. Goyal, L. D. Jackel, M. Monfort, U. Muller, J. Zhang *et al.*, "End to end learning for self-driving cars," *arXiv preprint arXiv:1604.07316*, 2016.
- [13] W. Yu, J. Peng, Q. Qiu, H. Wang, L. Zhang, and J. Ji, "Pathrl: An end-to-end path generation method for collision avoidance via deep reinforcement learning," *CoRR*, vol. abs/2310.13295, 2023.
- [14] S. Hu, L. Chen, P. Wu, H. Li, J. Yan, and D. Tao, "St-p3: End-to-end vision-based autonomous driving via spatial-temporal feature learning," in *European Conference on Computer Vision*. Springer, 2022, pp. 533–549.
- [15] Y. Hu, J. Yang, L. Chen, K. Li, C. Sima, X. Zhu, S. Chai, S. Du, T. Lin, W. Wang, L. Lu, X. Jia, Q. Liu, J. Dai, Y. Qiao, and H. Li, "Planning-oriented autonomous driving," in *IEEE/CVF Conference on Computer Vision and Pattern Recognition*, 2023.
- [16] K. Chitta, A. Prakash, and A. Geiger, "Neat: Neural attention fields for end-to-end autonomous driving," in *Proceedings of the IEEE/CVF International Conference on Computer Vision*, 2021, pp. 15 793–15 803.
- [17] A. Dosovitskiy, G. Ros, F. Codevilla, A. Lopez, and V. Koltun, "Carla: An open urban driving simulator," in *Conference on robot learning*. PMLR, 2017, pp. 1–16.
- [18] Y. Zhang, Z. Lu, X. Zhang, J.-H. Xue, and Q. Liao, "Deep learning in lane marking detection: A survey," *IEEE Transactions on Intelligent Transportation Systems*, vol. 23, no. 7, pp. 5976–5992, 2022.
- [19] H. Wang, C. Wang, C. Chen, and L. Xie, "F-LOAM : Fast lidar odometry and mapping," in *IEEE/RSJ International Conference on Intelligent Robots and Systems, IROS 2021, Prague, Czech Republic, September 27 - Oct. 1, 2021*. IEEE, 2021, pp. 4390–4396. [Online]. Available: <https://doi.org/10.1109/IROS51168.2021.9636655>
- [20] Y. Duan, J. Peng, Y. Zhang, J. Ji, and Y. Zhang, "Pfilter: Building persistent maps through feature filtering for fast and accurate lidar-based SLAM," in *IEEE/RSJ International Conference on Intelligent Robots and Systems, IROS 2022, Kyoto, Japan, October 23-27, 2022*. IEEE, 2022, pp. 11 087–11 093.
- [21] J. Lin and F. Zhang, "Loam livox: A fast, robust, high-precision lidar odometry and mapping package for lidars of small fov," in *2020 IEEE International Conference on Robotics and Automation, ICRA 2020, Paris, France, May 31 - August 31, 2020*. IEEE, 2020, pp. 3126–3131. [Online]. Available: <https://doi.org/10.1109/ICRA40945.2020.9197440>
- [22] T. Wang, X. Zhu, J. Pang, and D. Lin, "FCOS3D: fully convolutional one-stage monocular 3d object detection," in *IEEE/CVF International Conference on Computer Vision Workshops, ICCVW 2021, Montreal, BC, Canada, October 11-17, 2021*. IEEE, 2021, pp. 913–922.
- [23] Y. Li, J. Deng, Y. Zhang, J. Ji, H. Li, and Y. Zhang, "Ezfusion: A close look at the integration of lidar, millimeter-wave radar, and camera for accurate 3d object detection and tracking," *IEEE Robotics Autom. Lett.*, vol. 7, no. 4, pp. 11 182–11 189, 2022.
- [24] X. Chu, J. Deng, Y. Zhao, J. Ji, Y. Zhang, H. Li, and Y. Zhang, "Oa-bev: Bringing object awareness to bird's-eye-view representation for multi-camera 3d object detection," *arXiv preprint arXiv:2301.05711*, 2023.
- [25] X. Chu, J. Deng, Y. Li, Z. Yuan, Y. Zhang, J. Ji, and Y. Zhang, "Neighbor-vote: Improving monocular 3d object detection through neighbor distance voting," in *Proceedings of the 29th ACM International Conference on Multimedia*, 2021, pp. 5239–5247.
- [26] N. Garnett, R. Cohen, T. Pe'er, R. Lahav, and D. Levi, "3d-lanenet: end-to-end 3d multiple lane detection," in *Proceedings of the IEEE/CVF International Conference on Computer Vision*, 2019, pp. 2921–2930.
- [27] B. Liao, S. Chen, X. Wang, T. Cheng, Q. Zhang, W. Liu, and C. Huang, "Maptr: Structured modeling and learning for online vectorized HD map construction," in *The Eleventh International Conference on Learning Representations, ICLR 2023, Kigali, Rwanda, May 1-5, 2023*. OpenReview.net, 2023. [Online]. Available: [https://openreview.net/pdf?id=k7p\\_YAO7yE](https://openreview.net/pdf?id=k7p_YAO7yE)
- [28] T. Li, P. Jia, and *et al.*, "Lanesegnet: Map learning with lane segment perception for autonomous driving," *ICLR*, 2024.
- [29] C. Urmson and R. Simmons, "Approaches for heuristically biasing rrt growth," in *Proceedings 2003 IEEE/RSJ International Conference on Intelligent Robots and Systems (IROS 2003)(Cat. No. 03CH37453)*, vol. 2. IEEE, 2003, pp. 1178–1183.
- [30] J. J. Kuffner and S. M. LaValle, "Rrt-connect: An efficient approach to single-query path planning," in *Proceedings 2000 ICRA. Millennium Conference. IEEE International Conference on Robotics and Automation. Symposia Proceedings (Cat. No. 00CH37065)*, vol. 2. IEEE, 2000, pp. 995–1001.
- [31] M. Kleinbort, K. Solovey, Z. Littlefield, K. E. Bekris, and D. Halperin, "Probabilistic completeness of rrt for geometric and kinodynamic planning with forward propagation," *IEEE Robotics and Automation Letters*, vol. 4, no. 2, pp. x–xvi, 2018.
- [32] P. E. Hart, N. J. Nilsson, and B. Raphael, "A formal basis for the heuristic determination of minimum cost paths," *IEEE transactions on Systems Science and Cybernetics*, vol. 4, no. 2, pp. 100–107, 1968.
- [33] F. Codevilla, E. Santana, A. M. López, and A. Gaidon, "Exploring the limitations of behavior cloning for autonomous driving," in *Proceedings of the IEEE/CVF International Conference on Computer Vision*, 2019, pp. 9329–9338.
- [34] D. Chen, B. Zhou, V. Koltun, and P. Krähenbühl, "Learning by cheating," in *Conference on Robot Learning*. PMLR, 2020, pp. 66–75.
- [35] A. Amini, G. Rosman, S. Karaman, and D. Rus, "Variational end-to-end navigation and localization," in *2019 International Conference on Robotics and Automation (ICRA)*. IEEE, 2019, pp. 8958–8964.
- [36] D. Chen, V. Koltun, and P. Krähenbühl, "Learning to drive from a world on rails," in *Proceedings of the IEEE/CVF International Conference on Computer Vision*, 2021, pp. 15 590–15 599.
- [37] H. Shao, L. Wang, R. Chen, H. Li, and Y. Liu, "Safety-enhanced autonomous driving using interpretable sensor fusion transformer," in *Conference on Robot Learning*. PMLR, 2023, pp. 726–737.
- [38] D. Chen and P. Krähenbühl, "Learning from all vehicles," in *Proceedings of the IEEE/CVF Conference on Computer Vision and Pattern Recognition*, 2022, pp. 17 222–17 231.
- [39] A. Prakash, K. Chitta, and A. Geiger, "Multi-modal fusion transformer for end-to-end autonomous driving," in *Proceedings of the IEEE/CVF Conference on Computer Vision and Pattern Recognition*, 2021, pp. 7077–7087.
- [40] Z. Zhang, A. Liniger, D. Dai, F. Yu, and L. Van Gool, "End-to-end urban driving by imitating a reinforcement learning coach," in *Proceedings of the IEEE/CVF international conference on computer vision*, 2021, pp. 15 222–15 232.
- [41] K. Chitta, A. Prakash, B. Jaeger, Z. Yu, K. Renz, and A. Geiger, "Transfuser: Imitation with transformer-based sensor fusion for autonomous driving," *IEEE Transactions on Pattern Analysis and Machine Intelligence*, 2022.
- [42] B. Jiang, S. Chen, Q. Xu, B. Liao, J. Chen, H. Zhou, Q. Zhang, W. Liu, C. Huang, and X. Wang, "VAD: vectorized scene representation for efficient autonomous driving," in *IEEE/CVF International Conference on Computer Vision, ICCV 2023, Paris, France, October 1-6, 2023*. IEEE, 2023, pp. 8306–8316. [Online]. Available: <https://doi.org/10.1109/ICCV51070.2023.00766>
- [43] K. He, X. Zhang, S. Ren, and J. Sun, "Deep residual learning for image recognition," in *IEEE Conference on Computer Vision and Pattern Recognition, CVPR, Las Vegas, NV, USA, June 27-30, 2016*. IEEE.
- [44] T. M. Vu, R. Moezzi, J. Cyrus, and J. Hlava, "Model predictive control for autonomous driving vehicles," *Electronics*, vol. 10, no. 21, 2021.
- [45] T.-Y. Lin, P. Goyal, R. Girshick, K. He, and P. Dollár, "Focal loss for dense object detection," in *Proceedings of the IEEE international conference on computer vision*, 2017, pp. 2980–2988.
- [46] R. Girshick, "Fast r-cnn," in *Proceedings of the IEEE international conference on computer vision*, 2015, pp. 1440–1448.